

# Strange Stars with a Density-Dependent Bag Parameter

Nirvikar Prasad\* and R. S. Bhalerao†

*Tata Institute of Fundamental Research,  
Homi Bhabha Road, Colaba, Mumbai 400 005, India*

(Dated: January 23, 2004)

## Abstract

We have studied strange quark stars in the framework of the MIT bag model, allowing the bag parameter  $B$  to depend on the density of the medium. We have also studied the effect of Cooper pairing among quarks, on the stellar structure. Comparison of these two effects shows that the former is generally more significant. We studied the resulting equation of state of the quark matter, stellar mass-radius relation, mass-central-density relation, radius-central-density relation, and the variation of the density as a function of the distance from the centre of the star. We found that the density-dependent  $B$  allows stars with larger masses and radii, due to stiffening of the equation of state. Interestingly, certain stellar configurations are found to be possible only if  $B$  depends on the density. We have also studied the effect of variation of the superconducting gap parameter on our results.

PACS numbers: 26.60.+c, 97.60.Jd, 12.39.Ba, 97.10.Nf, 97.10.Pg

Keywords: neutron star, quark star, bag model, colour superconductivity

---

\*Electronic address: nirvikar@mailhost.tifr.res.in

†Electronic address: bhalerao@theory.tifr.res.in

## I. INTRODUCTION

The conjecture that the true ground state of quantum chromodynamics (QCD) may be the strange quark matter (SQM) was first explicitly stated by Witten [1], though various forms of quark matter had been considered earlier [2, 3]. The key idea is that the energy per baryon of SQM could be less than that of even  $^{56}\text{Fe}$ , the most stable nucleus, making SQM comparatively more stable. Farhi and Jaffe [4] studied SQM in the framework of the MIT bag model [5], for various values of the strange quark mass ( $m_s$ ) and the bag constant ( $B$ ). They found a “window of stability” in the  $m_s$ - $B$  plane inside which SQM was stable. The astrophysical implication of the stability of SQM, namely the possible existence of strange (quark) stars, was studied by Haensel *et al.* [6] and Alcock *et al.* [7]. They found that very compact strange stars are possible, which are much smaller than the normal neutron stars, the reason being that the strange stars are self-bound and generically different from the gravitationally bound stars. Of course, the actual existence of strange stars can only be confirmed by observational studies of pulsars and pulsar-like compact stars, including X-ray pulsars, X-ray bursters, anomalous X-ray pulsars, soft  $\gamma$ -ray repeaters and isolated neutron stars.

The SQM hypothesis has been around for almost two decades. Recent theoretical progress in our understanding of the cold and dense QCD matter has renewed the interest in this hypothesis: At low temperatures and sufficiently high baryon number densities, it is thought that quarks near the Fermi surface form Cooper pairs and new condensates develop. This is expected to lead to a colour-superconducting phase in the QCD phase diagram [8, 9]. Among the various colour-superconducting phases, the colour-flavour-locked (CFL) phase [10, 11, 12] is the one in which quarks of all three colours and all three flavours ( $u$ ,  $d$ ,  $s$ ) pair. Electrical neutrality of bulk CFL matter is ensured due to the fact that this phase favours equal number densities of  $u$ ,  $d$  and  $s$  quarks, despite their unequal masses [13, 14]. This also means that electrons are absent in the bulk CFL matter. Strange stars made of CFL matter seem to be favoured over those made of another colour-superconducting phase, namely the 2SC phase [15]. These theoretical developments have important implications for the existence of quark stars and neutron stars with quark cores.

Other reasons for the revival of interest in this area are the recent claims of observation of both mass and radius of compact stars [16, 17]. Although these claims are somewhat

controversial [18], they have further stimulated theoretical activity in this area.

The stability of SQM in the light of the above theoretical developments, and the structure of strange stars have recently been investigated by Lugones and Horvath [19, 20]. While constructing the equation of state (EOS) of the CFL matter, they introduced the vacuum energy by means of the phenomenological bag constant  $B$ . However, in view of the high densities encountered in neutron stars and quark stars, the question whether the bag constant should be held fixed at its free-space value or whether its variation with the density of the medium should be taken into account becomes very relevant. In this work, we investigate the effect of a density-dependent  $B$ , on the EOS and the resulting structure of the CFL strange stars.

The paper is organized as follows. In Sec. II we discuss various models of  $B(\rho)$  where  $\rho$  is the baryon number density of the medium. In Sec. III we consider the CFL matter and its EOS. Our numerical results for the resulting stellar structure are given in Sec. IV. In Sec. V we present our conclusions.

## II. DENSITY-DEPENDENT BAG PARAMETER

Of the many models of the nucleon that have been constructed so far, one of the most useful is the MIT Bag Model [5]: The nucleon is assumed to be a “bubble” of perturbative vacuum immersed in the non-perturbative or true vacuum, and quarks are confined to the bubble by means of a net inward pressure  $B$  exerted on it by the surrounding vacuum. The bag model has also been used to study the thermodynamics of the deconfinement phase transition. As the temperature rises above the deconfinement temperature, there is no difference between the two vacua, and the net inward pressure  $B$  must vanish. In other words,  $B$  must be viewed as a temperature-dependent quantity [21]. The analogy between the bag constant  $B$  and the condensation energy in the Nambu–Jona-Lasinio (NJL) model at finite temperature was pointed out in Ref. [22]. It was shown that as the temperature rises, this condensation energy decreases and goes to zero at the transition temperature. This provides a model of the temperature-dependent  $B$ . Density dependence of  $B$  can be motivated in an analogous manner: Since the deconfinement and the concomitant vanishing of  $B$  can also be brought about by raising the baryon number density  $\rho$ ,  $B$  should be treated as a density-dependent quantity [23].

There have been a number of attempts in the literature to evaluate the density dependence of  $B$ . The results, however, are model dependent, and no consensus seems to have emerged. In this work, we made use of the results of the following three studies published recently: (a) Liu *et al.* [24] extended the global colour symmetry model [25] to finite quark number chemical potentials  $\mu$ , in order to derive the variation of  $B$  with  $\mu$  and  $\rho$ . (b) Burgio *et al.* [26] used the CERN SPS data on heavy-ion collisions to justify and determine the density dependence of  $B$ . (c) Aguirre [27, 28] used the NJL model to study the modification of the QCD vacuum with increasing baryonic density and to extract the medium dependence of  $B$ .

(a) Since Liu *et al.* have not presented their  $B(\rho)$  or  $B(\mu)$  in a parametric form, we have fitted their results with a suitable analytic expression with two parameters  $a_1$  and  $a_2$ :

$$B(\rho)/B(0) = \exp[-(a_1x^2 + a_2x)], \quad (1)$$

where  $x \equiv \rho/\rho_0$  is the normalized baryon number density,  $\rho_0$  is the baryon number density of the ordinary nuclear matter,  $a_1 = 0.0125657$ , and  $a_2 = 0.29522$ . They took  $B(0) = 114 \text{ MeV/fm}^3 = (172 \text{ MeV})^4$ . (b) Burgio *et al.* have presented their  $B(\rho)$  in a parametric form:

$$B(\rho) = B_{as} + (B_o - B_{as}) \exp(-\beta x^2), \quad (2)$$

where  $B_{as} = 38 \text{ MeV/fm}^3$ ,  $B_o = 200 \text{ MeV/fm}^3 = (198 \text{ MeV})^4$ ,  $\beta = 0.14$ , and  $x$  is as defined above. (c) Aguirre [28] has calculated  $B(\rho)$  for a symmetric  $uds$  quark matter relevant for a CFL quark star. His  $B(\rho)$ , in  $\text{MeV/fm}^3$ , is given by

$$\begin{aligned} B(\rho) &= a + b_1x + b_2x^2 + b_3x^3 + b_4x^4 + b_5x^5, \quad x \leq 9 \\ &= \beta \exp(-\alpha(x - 9)), \quad x > 9 \end{aligned} \quad (3)$$

where  $x$  is as defined earlier. Further,  $a = 291.59096$ ,  $b_1 = -142.25581$ ,  $b_2 = 39.29997$ ,  $b_3 = -6.04592$ ,  $b_4 = 0.46817$ ,  $b_5 = -0.01421$ ,  $\alpha = 0.253470705$ , and  $\beta = 19.68764$ . Thus in this case  $B(0) = 291.59096 \text{ MeV/fm}^3 = (217.6 \text{ MeV})^4$ .

We display, in Fig. 1,  $B(\rho)$  vs  $\rho$  corresponding to Eqs. (1)-(3). These three models provide  $B(\rho)$  over a sufficiently wide range of densities expected to be seen inside quark stars. Secondly, the above three values of  $B(0)$  span more or less the whole range of values of the bag constant found in the literature. Finally, as is clear from Eqs. (1)-(3), they yield qualitatively different shapes for  $B(\rho)$ : (1) and (3) have negative slopes at  $x = 0$ , while (2)

has a vanishing slope; (1) and (3) vanish as  $x \rightarrow \infty$ , while (2) tends to a positive constant. It will be interesting to investigate what effects these different shapes and magnitudes of  $B(\rho)$  have on the EOS and the stellar structure. We shall use these three models in subsequent sections; all our numerical results are labeled accordingly as (a), (b), or (c).

### III. THERMODYNAMICS OF THE CFL PHASE

The free energy density  $\Omega_{CFL}$  of the CFL phase, at temperature  $T = 0$ , is obtained as follows [13]. We first consider the free energy density  $\Omega_{free}$  of an unpaired quark matter in which all quarks that are “going to pair” have a common Fermi momentum  $\nu$ : the CFL pairing is most effective if the Fermi momenta of the  $u$ ,  $d$ , and  $s$  flavours are the same. Although the nonzero strange quark mass tends to favour unequal number densities for the three flavours, the CFL pairing forces the three flavours to have the same Fermi momentum and hence the same number density, so long as  $m_s$  is not too large. If  $\Delta$  is the colour-superconductivity gap parameter and  $\mu$  is the quark number chemical potential, then the binding energy of the  $qq$  Cooper pairs can be included (to leading order in  $\Delta/\mu$ ) by subtracting  $3\Delta^2\mu^2/\pi^2$  from  $\Omega_{free}$ . The vacuum energy density in the presence of a finite chemical potential  $\mu$ , is included by adding  $B(\mu)$ . This gives

$$\begin{aligned}\Omega_{CFL} &= \Omega_{free} - \frac{3}{\pi^2}\Delta^2\mu^2 + B(\mu) \\ &= \frac{6}{\pi^2} \int_0^\nu (p - \mu)p^2 dp + \frac{3}{\pi^2} \int_0^\nu [(p^2 + m_s^2)^{1/2} - \mu]p^2 dp - \frac{3}{\pi^2}\Delta^2\mu^2 + B(\mu),\end{aligned}\quad (4)$$

see [29, 30] which, however, treat  $B$  as a constant. The baryon number density  $\rho = -\partial\Omega_{CFL}/(3\partial\mu)$  and particle number densities for individual flavours are given by

$$\rho = n_u = n_d = n_s = \frac{(\nu^3 + 2\Delta^2\mu)}{\pi^2} - \frac{1}{3}B'(\mu),\quad (5)$$

where  $B'(\mu) \equiv dB/d\mu$ . The common Fermi momentum  $\nu$  is chosen to minimize the free energy density with respect to a variation in  $\nu$ . This gives

$$\nu = 2\mu - \left(\mu^2 + \frac{m_s^2}{3}\right)^{1/2}.\quad (6)$$

Energy density of the CFL matter is given by

$$\varepsilon = \sum_i \mu_i n_i + \Omega_{CFL} = 3\mu\rho - P,\quad (7)$$

since  $\mu = (\mu_u + \mu_d + \mu_s)/3$  and the pressure  $P$  is given by  $P = -\Omega_{CFL}$ .

Now we obtain the equation of state of the CFL matter, in the standard form. Integrations in Eq. (4) can be performed in a straightforward manner and we get

$$\Omega_{free} = \frac{3\nu^4}{2\pi^2} - \frac{3\mu\nu^3}{\pi^2} + \frac{3}{\pi^2} \left[ \frac{\nu}{4}(m_s^2 + \nu^2)^{3/2} - \frac{m_s^2\nu}{8}(m_s^2 + \nu^2)^{1/2} - \frac{m_s^4}{8} \sinh^{-1} \frac{\nu}{m_s} \right]. \quad (8)$$

We are interested in the region where  $m_s$  is small compared to the chemical potential  $\mu$ . So it is sufficient to keep terms up to order  $m_s^4$  in  $\Omega_{free}$  [15]. To that end, first note that the common Fermi momentum  $\nu$  (Eq. (6)) is given by

$$\nu = \mu - \frac{m_s^2}{6\mu} + \frac{m_s^4}{72\mu^3}, \quad (9)$$

where we have kept terms up to order  $m_s^4$ . This yields

$$\Omega_{CFL} = \frac{-3\mu^4}{4\pi^2} + \frac{3m_s^2\mu^2}{4\pi^2} - \frac{1 - 12 \log(m_s/2\mu)}{32\pi^2} m_s^4 - \frac{3}{\pi^2} \Delta^2 \mu^2 + B(\mu). \quad (10)$$

Substitution of  $\nu$  given by Eq. (9), in Eqs. (5) and (7) yields

$$\rho = \frac{\mu^3}{\pi^2} - \frac{m_s^2\mu}{2\pi^2} + \frac{m_s^4}{8\pi^2\mu} + \frac{2}{\pi^2} \Delta^2 \mu - \frac{1}{3} B'(\mu), \quad (11)$$

$$\varepsilon = \frac{9\mu^4}{4\pi^2} - \frac{3m_s^2\mu^2}{4\pi^2} + \frac{11m_s^4}{32\pi^2} + \frac{3 \log(m_s/2\mu)}{8\pi^2} m_s^4 + \frac{3}{\pi^2} \Delta^2 \mu^2 + B(\mu) - \mu B'(\mu). \quad (12)$$

The pressure is given by

$$P = \frac{3\mu^4}{4\pi^2} - \frac{3m_s^2\mu^2}{4\pi^2} + \frac{1 - 12 \log(m_s/2\mu)}{32\pi^2} m_s^4 + \frac{3}{\pi^2} \Delta^2 \mu^2 - B(\mu). \quad (13)$$

Equations (12) and (13) give  $\varepsilon$  and  $P$  in terms of  $\mu$  as a parameter. The EOS in the standard form can be obtained from these two equations and it reads

$$\varepsilon = 3P + 4B(\mu) - \frac{6\Delta^2\mu^2}{\pi^2} + \frac{3m_s^2\mu^2}{2\pi^2} + \frac{1 + 6 \log(m_s/2\mu)}{4\pi^2} m_s^4 - \mu B'(\mu). \quad (14)$$

If only the first two terms on the rhs of Eq. (14) are kept then it reduces to the ideal gas EOS in the bag model. The occurrence of the pairing term stiffens the EOS because we get a higher pressure at the same energy density. A nonzero value of  $m_s$ , on the other hand, tends to reduce the pressure leading to a softer EOS.

If Eq. (14) is to be used to study the stellar structure, one needs to know  $B(\mu)$  and its derivative  $B'(\mu)$ . In Sec. II, we have described three models of  $B(\rho)$ . Consider first the

model of Liu *et al.* [24], denoted by (a) in Sec. II. Their formalism in fact first yields  $B(\mu)$ , not  $B(\rho)$ . They, however, do not present their numerical results for  $B(\mu)$ . Instead, they use the relation  $\rho = 2\mu^3/(3\pi^2)$  to obtain  $B(\rho)$  and present numerical results for  $B(\rho)$ . In order to extract their  $B(\mu)$ , we have to use exactly the same relation between  $\rho$  and  $\mu$ . This is how we obtained  $B(\mu)$  in the case of the model (a). Next, consider the models (b) and (c) of Sec. II. To obtain  $B(\mu)$  from  $B(\rho)$  in these cases, we proceed as follows. Consider Eq. (11). It can be rewritten as

$$\rho = f(\mu) - \frac{1}{3} \frac{dB}{d\mu}, \quad (15)$$

where  $f(\mu)$  denotes the sum of the first four terms on the rhs of Eq. (11). In the case of model (b), Eq. (2) can be inverted to get  $\rho(B)$  which can be substituted in Eq. (15). This gives a first-order differential equation between  $B$  and  $\mu$ , which can be solved numerically. In the case of model (c), it is easier to eliminate  $B$  between Eqs. (3) and (15), and the resulting differential equation looks like

$$\frac{dx}{d\mu} = 3[f(\mu) - \rho_0 x]/(dB/dx). \quad (16)$$

In both the cases, the initial condition necessary to solve the differential equation is obtained from the fact that for sufficiently large  $\mu$ ,  $dB/d\mu$  is nearly zero. We have checked the solutions of the above differential equations by substituting them in the original equations (Eqs. (15) and (2) in the case of model (b), and Eqs. (15) and (3) in the case of model (c)).

Before we display our results for the EOS, Eq. (14), it is useful to see how the quantities  $B$ ,  $B'$ ,  $\varepsilon$  in Eq. (12), and  $P$  in Eq. (13) vary with  $\mu$ . This is shown in Fig. 2. Consider first  $B(\mu)$ . Its broad features are in agreement with those of  $B(\rho)$  seen in Fig. 1. Also note that in spite of the large differences among the values of  $B(\rho = 0)$  corresponding to the three models, the curves for  $B(\mu)$  in the region relevant to quark stars ( $\mu \sim$  a few hundred MeV) do not differ drastically from each other. Consider next  $B'(\mu)$ . It is either negative or zero depending on the value of  $\mu$ . We have plotted  $|\mu B'(\mu)|$  since it occurs in Eq. (12). This quantity obviously tends to vanish at very small and very large values of  $\mu$ , and it displays a gentle peak at an intermediate value of  $\mu$ .  $\varepsilon(\mu)$  contains  $|\mu B'(\mu)|$ , whereas  $P(\mu)$  does not. However, because of the relatively small magnitude of  $|\mu B'(\mu)|$ , the curves for  $\varepsilon(\mu)$  and  $P(\mu)$  have similar shapes. Interestingly, the magnitudes of  $\varepsilon(\mu)$  and  $P(\mu)$  are seen to be insensitive to the details of the three models of  $B(\rho)$ . Finally, note that  $P(\mu)$  is positive only when  $\mu$  exceeds a certain threshold value.

Figure 3 displays the EOS of the CFL matter and unpaired quark matter, in the various models considered above. It is easy to understand the shapes of these curves by looking at  $P(\mu)$  and  $\varepsilon(\mu)$  in Fig. 2, and noting that Fig. 3 is obtained essentially by eliminating  $\mu$ . Some general trends emerge: (1) If  $B$  is treated as a constant independent of the density of the medium then the EOS appears to be linear; see the dashed lines in Fig. 3. On the other hand, if  $B$  depends on  $\mu$ , the EOS is slightly nonlinear. (2) The pairing term is seen to make the EOS stiffer, so does the density dependent  $B$ . However, the latter effect is seen to be more significant. This will be corroborated further when we present the stellar structure curves in the next section.

We now discuss the issue of the “window of stability”. This is the region in the  $m_s$ - $B$  plane, in which the SQM has energy per baryon ( $\varepsilon/\rho$ ) less than 939 MeV, and which was first discussed in Ref. [4]. Since both  $m_s$  and  $B$  tend to increase  $\varepsilon/\rho$ , this region obviously lies near small values of  $m_s$  and  $B$ , in the first quadrant of the  $m_s$ - $B$  plane. It is bounded on the left by the vertical line  $B = 57 \text{ MeV/fm}^3 = (145 \text{ MeV})^4$ , and on the other side, by the  $\varepsilon/\rho = 939 \text{ MeV}$  contour. The boundary on the left arises because if  $B$  were smaller than 57 MeV/fm<sup>3</sup>, i.e., if the inward pressure holding the quarks together in the nucleon were too small (see Sec. II), the nucleon and hence the nuclei would have dissolved into  $ud$  quark matter. Since that does not happen,  $B$  must not be smaller than 57 MeV/fm<sup>3</sup>.

Recently, it was shown that the window of stability is enlarged considerably if the SQM undergoes a phase transition to a CFL quark matter [19]. The enlargement occurs because the  $\varepsilon/\rho = 939 \text{ MeV}$  contour gets shifted to the right. Let us understand this. To probe the absolute stability of the SQM, we need to set the external pressure  $P$  equal to zero. Then Eqs. (7) and (10) yield, respectively,

$$\varepsilon/\rho = 3\mu, \tag{17}$$

and

$$\frac{-3\mu^4}{4\pi^2} + \frac{3m_s^2\mu^2}{4\pi^2} - \frac{3}{\pi^2}\Delta^2\mu^2 + B(\mu) = 0, \tag{18}$$

where we have ignored the  $\mathcal{O}(m_s^4)$  term in Eq. (10), for simplicity. Ignoring the  $\mu$ -dependence of  $B$  as in [19] and eliminating  $\mu$  in the last two equations one gets  $\varepsilon/\rho$  as a function of  $m_s$ ,  $B$ , and  $\Delta$ . It is clear that a nonzero value of  $\Delta$  shifts the  $\varepsilon/\rho = 939 \text{ MeV}$  contour to the right thereby enlarging the window of stability. This is essentially because of the opposite signs of the  $B$ - and  $\Delta$ -terms in Eq. (18): The  $\Delta$ -term tends to nullify the effect of a large  $B$ .

The larger the  $\Delta$ , the larger the value of  $B$  one may have, while still maintaining  $\varepsilon/\rho < 939$  MeV. This is clearly borne out by the results of [19].

Let us now discuss how a  $\mu$ -dependent  $B$  would affect the window of stability. Earlier, when  $\Delta$  was introduced, the functional dependence of  $\varepsilon/\rho$  on  $m_s$  and  $B$  was changed (see Eqs. (17)-(18)), and hence the contour  $\varepsilon/\rho = 939$  MeV got shifted. Now, whether  $B$  is constant or  $\mu$ -dependent, the new functional dependence remains unchanged. In other words, the  $\varepsilon/\rho = 939$  MeV contour in the present work is the same as in [19]. We shall revisit the issue of the window of stability in the next section, when we discuss Fig. 4.

#### IV. STRUCTURE OF STRANGE STARS

The equations of stellar structure, namely the Tolman-Oppenheimer-Volkoff (TOV) equations [32, 33], give rise to a one-parameter family of stars corresponding to a particular equation of state: By specifying the central density as the parameter, one can numerically integrate the TOV equations, starting at the centre of the star and going radially outward until the pressure becomes zero which indicates that the surface of the star has been reached. This determines the radius  $R$  and the mass  $M$  of the star, for the specified central density. By choosing successively larger values of the central density, one can generate a sequence of stars of increasing mass. The sequence ends when any further increase in the central density leads to a star with a lower mass, which indicates an unstable configuration. This end-of-sequence star is the maximum-mass star for the sequence. For a given EOS, the mass-radius relationship is the most important property of the family of stars. This is because it can be compared directly with observational data in order to test and calibrate the theory. While both the mass and the radius are not known so far for any pulsar, a number of mass measurements exist and the data on the radius are getting better.

We now present our numerical results on the structure of the strange stars. We set the strange quark mass  $m_s = 150$  MeV and the gap parameter  $\Delta = 0$  or 100 MeV (except in Figs. 8 and 9 where we vary  $\Delta$  between 0 and 150 MeV). We recall from Ref. [19] that the stability of SQM requires that if  $m_s = 150$  MeV and  $\Delta = 100$  MeV, then the bag constant  $B$  should be less than about 117 MeV/fm<sup>3</sup>, and if  $m_s = 150$  MeV and  $\Delta = 0$ , then  $B$  should be less than about 77 MeV/fm<sup>3</sup>. Now consider the three models of the density-dependent  $B$ , described in Sec. II. Since  $B$  is a decreasing function of the baryon number density  $\rho$ ,

the above upper limits on the values of  $B$  necessarily imply lower limits on the values of  $\rho$ . In the numerical work, one has to ensure that these limits are satisfied, so that the resulting star is always within the window of stability.

We now discuss Figs. 4-9. In all these figures, dashed curves correspond to the case when  $B$  is taken as a constant independent of the density of the medium, while the solid curves correspond to the case when  $B$  varies with  $\rho$ , and the panels (a), (b), (c) refer to the three models of  $B(\rho)$ , described in Sec. II.

Figure 4 shows the mass-radius sequences. Consider first Fig. 4(a). Model (a) has  $B(0) = 114 \text{ MeV/fm}^3$  which is well within the window of stability if  $\Delta = 100 \text{ MeV}$  (see above). This allows us to draw the two curves labelled 100. *They show that a density-dependent  $B$  gives rise to larger and more massive stars.* If  $\Delta = 0$ , the above value of  $B(0)$  is outside the window. Hence there is no dashed curve labelled 0. However, the solid curve labelled 0 is allowed: Recall that the density cannot be arbitrarily small since the pressure needs to be positive (Fig. 2). Indeed, for any point on this curve, the density throughout the star is found to be high enough that  $B(\rho)$  is everywhere less than  $77 \text{ MeV/fm}^3$  (see above). *Interestingly, this sequence of stars has become possible only because we considered a density-dependent  $B$ .* Now consider Fig. 4(b). Model (b) has  $B(0) = 200 \text{ MeV/fm}^3$  which is outside the window of stability for both  $\Delta = 0$  and  $100 \text{ MeV}$ . Hence there are no dashed curves here. However, the solid curves labelled 0 and 100, are allowed because for any point on these curves, the density throughout the star is found to be high enough that  $B$  remains within the window of stability. Note again that these sequences of stars have become possible only because we considered a density-dependent  $B$ . Similar remarks can be made about Fig. 4(c). *Results in Fig. 4 seem to be robust — not very sensitive to the details of the three models of  $B(\rho)$  considered in this paper.*

The dot-dashed lines crossing the  $M$ - $R$  curves in Fig. 4 correspond to the  $M/M_\odot \simeq 0.15 R$  (in Km) constraint obtained by Cottam *et al.* [34] by using measurements of the red shift of spectral lines in X-ray bursts from EXO0748-676. In all Figs. 4(a-c) the crossing occurs at  $M/M_\odot \simeq 1.3$ - $1.4$ . *Thus the present calculation has been able to construct strange stars which are compatible with this constraint.*

It is a built-in feature of the TOV equations that the sequence of stars ends, whatever may be the EOS. The typical shape of the sequence shown in Fig. 4 ( $M \propto R^3$  approximately) is generic to compact stars that are self-bound. This is borne out by the fact that although

the EOS used here is quite different from that used in [6], [7] or [20], the shapes of the curves in Fig. 4 are similar to those obtained in the earlier studies.

Density-dependent  $B$  makes the EOS stiffer; see Fig. 3. A stiffer EOS can resist the collapse of a star to a black hole, to a greater extent. Hence stars with larger radii and masses result. What is true for an individual star holds also for a sequence of stars, which as a whole shifts toward larger mass and radius. This is evident in Fig. 4(a).

Further, since the EOS is not strictly linear, simple scaling where the mass and radius scale as  $1/\sqrt{B}$  no longer holds [31]. Actually when  $\mu$ -dependent  $B$  is considered, the meaning of scaling as such is lost because as one moves from the surface of a star toward its centre,  $B$  keeps decreasing. That is, no fixed value can be assigned to it.

Finally, in Fig. 4(a), note that the difference between the two curves labelled 100 is more significant than the difference between the two solid curves. Similar observations can be made about Figs. 5-7. *This underscores the importance of the modification of  $B$  in a dense medium vis-à-vis the phenomenon of Cooper pairing among quarks.*

We plot mass  $M$  vs central energy density  $\varepsilon_c$ , in Fig. 5. As  $\varepsilon_c$  rises, so does the mass, until a plateau is reached which leads to the end of the sequence. The slope  $dM/d\varepsilon_c$  is positive signifying stable configurations. Since the solid curves correspond to a stiffer EOS (Fig. 3), for a given value of the central energy density they represent more massive stars. Figure 6 shows the corresponding variation of the radius  $R$  with  $\varepsilon_c$ .

In Fig. 7 we show, for the maximum-mass star, the variation of the density with the distance  $r$  from the centre of the star. In the case of the density-dependent  $B$ , the EOS is stiffer (Fig. 3) and the central density is lower. In other words, the solid curve labelled 100 in Fig. 7(a) begins at a lower value of  $\rho/\rho_0$  than the dashed curve. In spite of this, the star in the former case is more massive because it has a larger radius, and the large- $r$  regions contribute to the mass in a dominant fashion.

We display the variation of the maximum mass with the gap parameter  $\Delta$ , in Fig. 8. The increase in mass with  $\Delta$  is expected because as  $\Delta$  increases the EOS becomes stiffer. Recall that in model (a),  $B(0) = 114 \text{ MeV/fm}^3$ . For this point to be inside the window of stability,  $\Delta$  has to be at least  $\sim 100 \text{ MeV}$ . Hence in Fig. 8(a) the dashed curve starts near  $\Delta = 100 \text{ MeV}$ . In Fig. 8(b) there is no dashed curve because in model (b),  $B(0) = 200 \text{ MeV/fm}^3$  which is not inside the window if  $\Delta \leq 150 \text{ MeV}$ . A similar remark can be made about Fig. 8(c). In Fig. 9 we plot the maximum radius vs  $\Delta$ . Recent data hint at the possibility of

very compact stars [16, 17]. A smaller and denser object in comparison to the neutron stars will be a strong candidate for a strange star.

## V. CONCLUSIONS

The fact that quarks normally exist in a confined state, does not automatically rule out the strange quark matter hypothesis. This hypothesis does not violate any physical principle and is also not ruled out by any observed phenomenon. The real difficulty in verifying the hypothesis lies in the fact that the underlying theory, namely the QCD at quark chemical potential ( $\mu$ ) of the order of several 100 MeV, is difficult to handle and does not yet allow a rigorous calculation. Unfortunately, the phenomenological models which one resorts to, give the energy per baryon of SQM very close to that of  $^{56}\text{Fe}$ . In view of the uncertainties and the approximations involved, it is difficult to make a definitive statement.

One way to make progress in this situation is to make the models more realistic. Taking the density dependence of  $B$  into account is a step in that direction.

1. We have shown that this has a significant effect on the equation of state of SQM and hence on the resulting stellar structure curves. Specifically, the density dependence of  $B$  leads to a stiffer EOS which gives rise to stars with larger masses and radii.
2. Our results for the  $M$ - $R$  curves do not depend sensitively on the details of the three models of the density dependence of  $B$  considered in this paper.
3. Effect of the newly discovered phenomenon of colour superconductivity on the structure of compact stars has been studied by several authors. An important point which emerges from the present work is that the results depend more sensitively on the density dependence of the bag parameter than on the phenomenon of Cooper pairing of the quarks.
4. Another observation that we made is with regard to the ‘window of stability’ of SQM. We showed that the density dependence of  $B$  does not affect the window.
5. We have been able to construct stars that are compatible with the constraint given in [34]. Moreover, their masses lie in the astrophysically plausible range.

6. Most importantly, certain stellar sequences which are ruled out by the requirement of the stability of SQM, if  $B$  is treated as a constant, are allowed if the density-dependence of  $B$  is taken into consideration.

There are a number of ways in which this work can be extended. As mentioned in Sec. III, we considered the pairing interaction to the leading order in  $\Delta/\mu$ . The same approximation was made also in Refs. [15, 19, 20, 29, 30]. Since  $\Delta/\mu$  can be as large as  $\sim 1/3$ , it is clearly desirable to go beyond this approximation. Secondly, the density dependence of  $\Delta$  and  $m_s$  can be included to get a more complete picture. (In the present work, we have varied  $\Delta$  over a wide range and studied how it affects our results. It appears that allowing  $\Delta$  to depend upon the density of the medium, may not change the results significantly. See, e.g., the two solid curves in Fig. 7(a), where we show the variation of the density as one goes from the center to the surface of the star. Each solid curve is for a *fixed* value of  $\Delta$ , namely 0 or 100 MeV. Obviously, curves for intermediate values of  $\Delta$  (say, 10, 20, ..., 90 MeV) would lie in between these two curves. Hence if  $\Delta$  were allowed to vary with the density or equivalently with  $r$ , the resulting curve is not expected to be drastically different from the two solid curves shown here.) Thirdly, existence of additional phases (like 2SC, crystalline, etc.) can be looked into. Finally, we did not include perturbative corrections to the equation of state; these can be incorporated. Furthermore, a similar study where the bag parameter is dependent on density can be made for hybrid stars.

We conclude by noting that the limitations of the present work, pointed out in the preceding paragraph, and the simplicity of the theoretical model employed, should be kept in mind while interpreting the numerical results presented here.

### **Acknowledgments**

N. Prasad acknowledges many helpful discussions with H.M. Antia and A. Ray.

- 
- [1] E. Witten, Phys. Rev. D **30**, 272 (1984).
- [2] A. R. Bodmer, Phys. Rev. D **4**, 1601 (1971).
- [3] S. A. Chin and A. K. Kerman, Phys. Rev. Lett. **43**, 1292 (1979).
- [4] E. Farhi and R. L. Jaffe, Phys. Rev. D **30**, 2379 (1984).
- [5] A. Chodos, R. L. Jaffe, K. Johnson, C. B. Thorn and V. F. Weisskopf, Phys. Rev. D **9**, 3471 (1974).
- [6] P. Haensel, J. L. Zdunik and R. Schaeffer, Astron. Astrophys. **160**, 121 (1986).
- [7] C. Alcock, E. Farhi and A. Olinto, Astrophys. J. **310**, 261 (1986).
- [8] M. G. Alford, K. Rajagopal and F. Wilczek, Phys. Lett. B **422**, 247 (1998) [arXiv:hep-ph/9711395].
- [9] R. Rapp, T. Schafer, E. V. Shuryak and M. Velkovsky, Phys. Rev. Lett. **81**, 53 (1998) [arXiv:hep-ph/9711396].
- [10] K. Rajagopal and F. Wilczek, arXiv:hep-ph/0011333.
- [11] M. G. Alford, J. Berges and K. Rajagopal, Nucl. Phys. B **558**, 219 (1999) [arXiv:hep-ph/9903502].
- [12] T. Schafer and F. Wilczek, Phys. Rev. D **60**, 074014 (1999) [arXiv:hep-ph/9903503].
- [13] K. Rajagopal and F. Wilczek, Phys. Rev. Lett. **86**, 3492 (2001) [arXiv:hep-ph/0012039].
- [14] A. W. Steiner, S. Reddy and M. Prakash, Phys. Rev. D **66**, 094007 (2002) [arXiv:hep-ph/0205201].
- [15] M. Alford and K. Rajagopal, JHEP **0206**, 031 (2002) [arXiv:hep-ph/0204001].
- [16] J. A. Pons, F. M. Walter, J. M. Lattimer, M. Prakash, R. Neuhauser and P. h. An, Astrophys. J. **564**, 981 (2002) [arXiv:astro-ph/0107404].
- [17] J. J. Drake *et al.*, Astrophys. J. **572**, 996 (2002) [arXiv:astro-ph/0204159].
- [18] F. M. Walter and J. Lattimer, Astrophys. J. **576**, L145 (2002) [arXiv:astro-ph/0204199].
- [19] G. Lugones and J. E. Horvath, Phys. Rev. D **66**, 074017 (2002) [arXiv:hep-ph/0211070].
- [20] G. Lugones and J. E. Horvath, Astron. Astrophys. **403**, 173 (2003). [arXiv:astro-ph/0211638].
- [21] B. Muller and J. Rafelski, Phys. Lett. B **101**, 111 (1981).
- [22] S. Li, R. S. Bhalerao and R. K. Bhaduri, Int. J. Mod. Phys. A **6**, 501 (1991).
- [23] H. Reinhardt and B. V. Dang, Phys. Lett. B **173**, 473 (1986).

- [24] Y.-x. Liu, D.-f. Gao and H. Guo, Nucl. Phys. A **695**, 353 (2001) [arXiv:hep-ph/0105202].
- [25] C. D. Roberts, R. T. Cahill and J. Praschifka, Ann. Phys. (NY) **188**, 20 (1988).
- [26] G. F. Burgio, M. Baldo, P. K. Sahu, A. B. Santra and H. J. Schulze, Phys. Lett. B **526**, 19 (2002) [arXiv:astro-ph/0111440].
- [27] R. Aguirre, Phys. Lett. B **559**, 207 (2003) [arXiv:nucl-th/0212020].
- [28] R. Aguirre, private communication.
- [29] M. Alford and S. Reddy, Phys. Rev. D **67**, 074024 (2003) [arXiv:nucl-th/0211046].
- [30] M. G. Alford, K. Rajagopal, S. Reddy and F. Wilczek, Phys. Rev. D **64**, 074017 (2001) [arXiv:hep-ph/0105009].
- [31] N.K. Glendenning, *Compact Stars – Nuclear Physics, Particle Physics, and General Relativity*, 2nd edn., (Springer-Verlag, Berlin, 2000).
- [32] R. Tolman, Phys. Rev. **55**, 364 (1939).
- [33] J. R. Oppenheimer and G. M. Volkoff, Phys. Rev. **55**, 374 (1939).
- [34] J. Cottam, F. Paerels and M. Mendez, Nature **420**, 51 (2002) [arXiv:astro-ph/0211126].

## Figure Captions

Fig. 1: Bag parameter  $B$  vs baryon number density  $\rho$  for the three models considered in this paper.

Fig. 2: Energy density  $\varepsilon$ , pressure  $P$ , bag parameter  $B$ , and  $|\mu dB/d\mu|$  vs quark number chemical potential  $\mu$ , for the gap parameter  $\Delta = 100$  MeV. Here and in the rest of the figures, the panels (a), (b), and (c) refer to the three models of the density-dependent bag parameter  $B(\rho)$ , described in Sec. II. (For the sake of clarity,  $B \times 5$  rather than  $B$  is plotted.)

Fig. 3: Pressure  $P$  vs energy density  $\varepsilon$ , i.e., the equation of state of the quark matter. In each panel, the two solid curves correspond to a calculation with a density-dependent  $B$ , and the two dashed curves correspond to a calculation with a constant  $B$ . Curves are labelled by the values of  $\Delta$  in MeV.

Fig. 4: Mass  $M$  (in units of the solar mass  $M_\odot$ ) vs radius  $R$  of a strange star. Notation as in Figs. 2 and 3. The dot-dashed line is the  $M/M_\odot \simeq 0.15 R$  (in Km) constraint obtained in Ref. [34].

Fig. 5: Mass  $M$  (in units of the solar mass  $M_\odot$ ) vs central energy density  $\varepsilon_c$  (in units of the energy density  $\varepsilon_0$  of the normal nuclear matter) of a strange star. Notation as in Figs. 2 and 3.

Fig. 6: Radius  $R$  vs central energy density  $\varepsilon_c$  (in units of the energy density  $\varepsilon_0$  of the normal nuclear matter) of a strange star. Notation as in Figs. 2 and 3.

Fig. 7: Baryon number density  $\rho$  (in units of the baryon number density  $\rho_0$  of the normal nuclear matter) vs distance  $r$ , for the maximum-mass strange star. Notation as in Figs. 2 and 3.

Fig. 8: The maximum mass  $M$  of a strange star (in units of the solar mass  $M_\odot$ ) vs the gap parameter  $\Delta$ . Notation as in Figs. 2 and 3.

Fig. 9: The maximum radius  $R$  of a strange star vs the gap parameter  $\Delta$ . Notation as in Figs. 2 and 3.

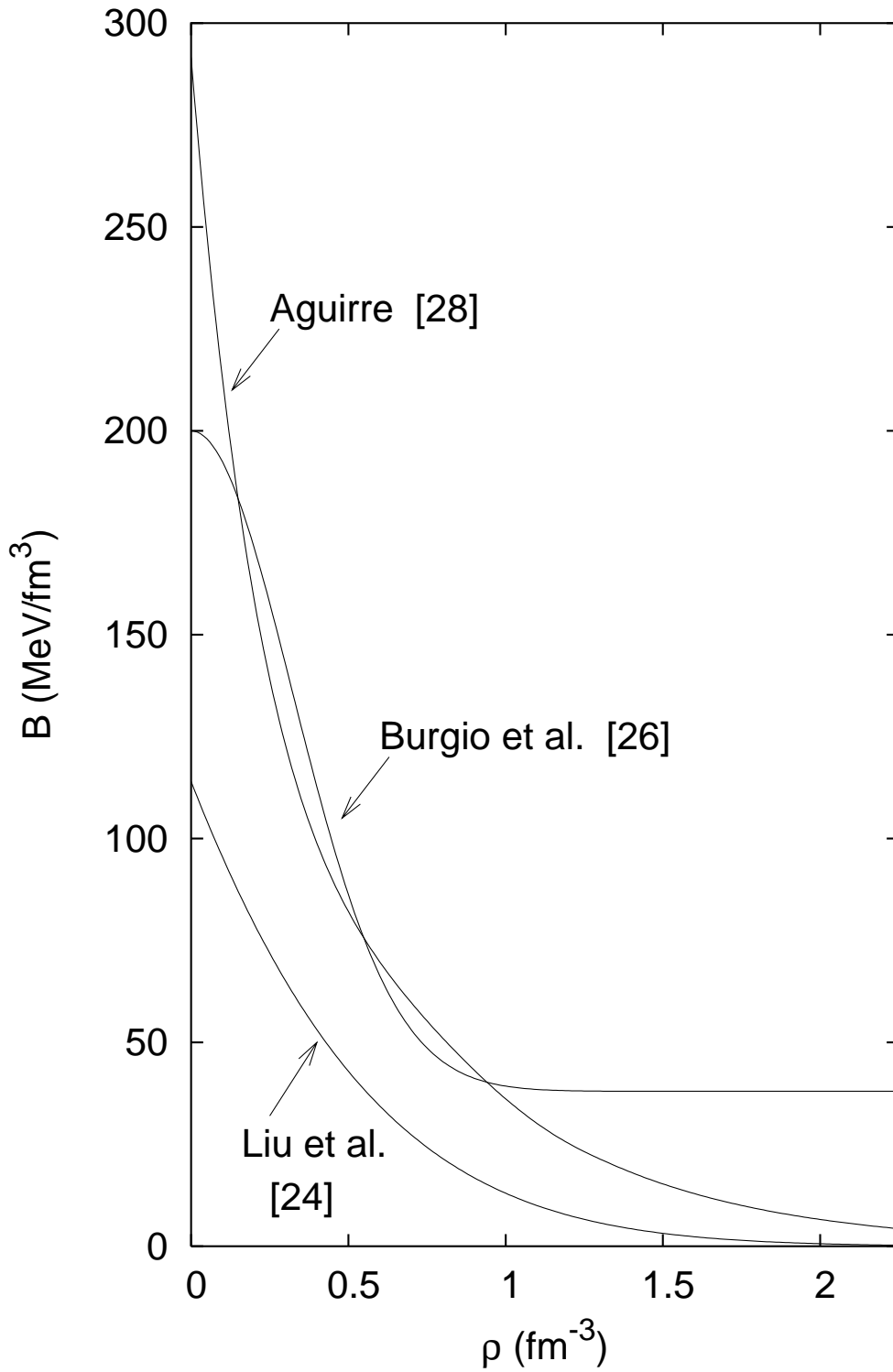


Fig. 1

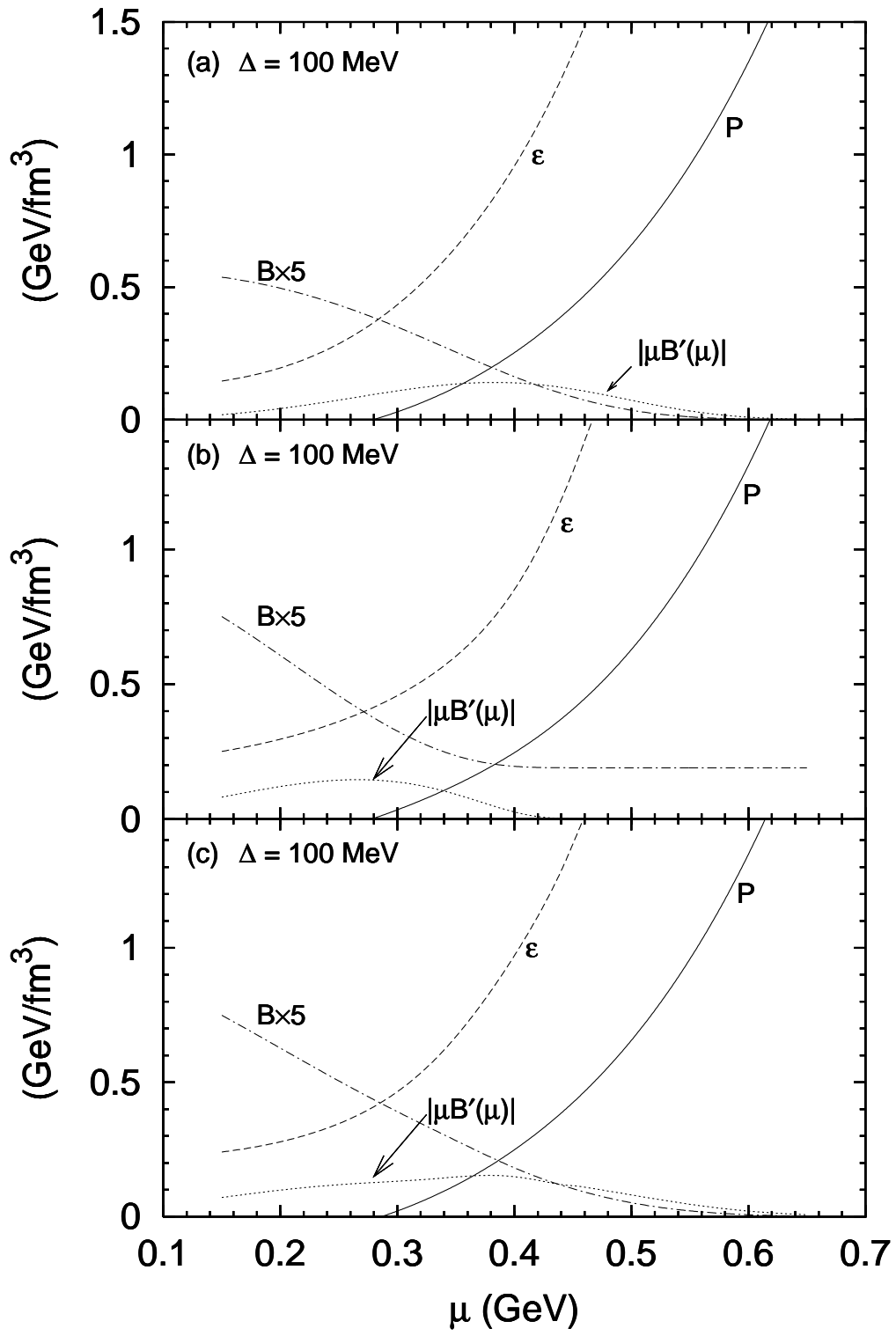


Fig. 2

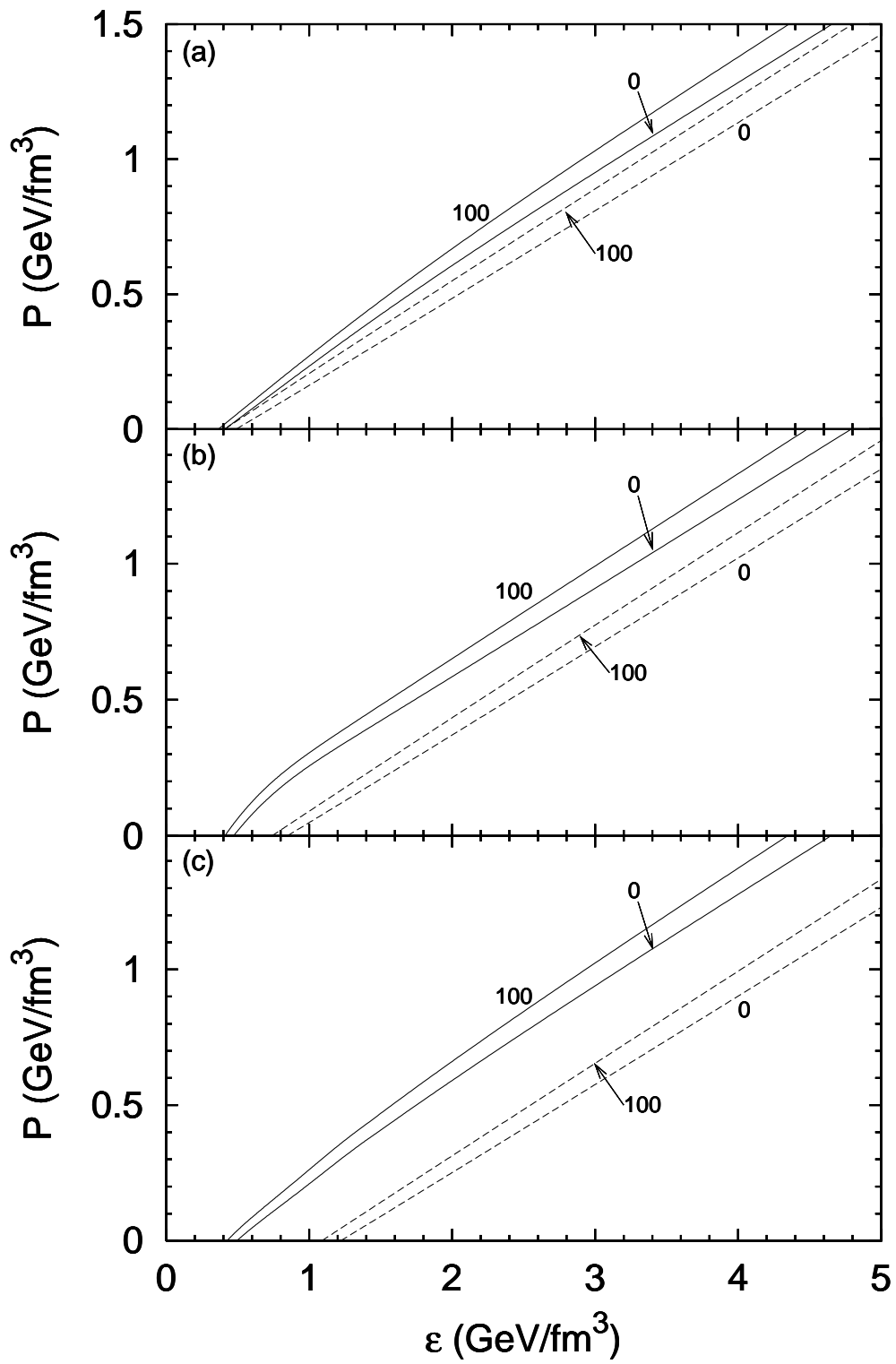


Fig. 3

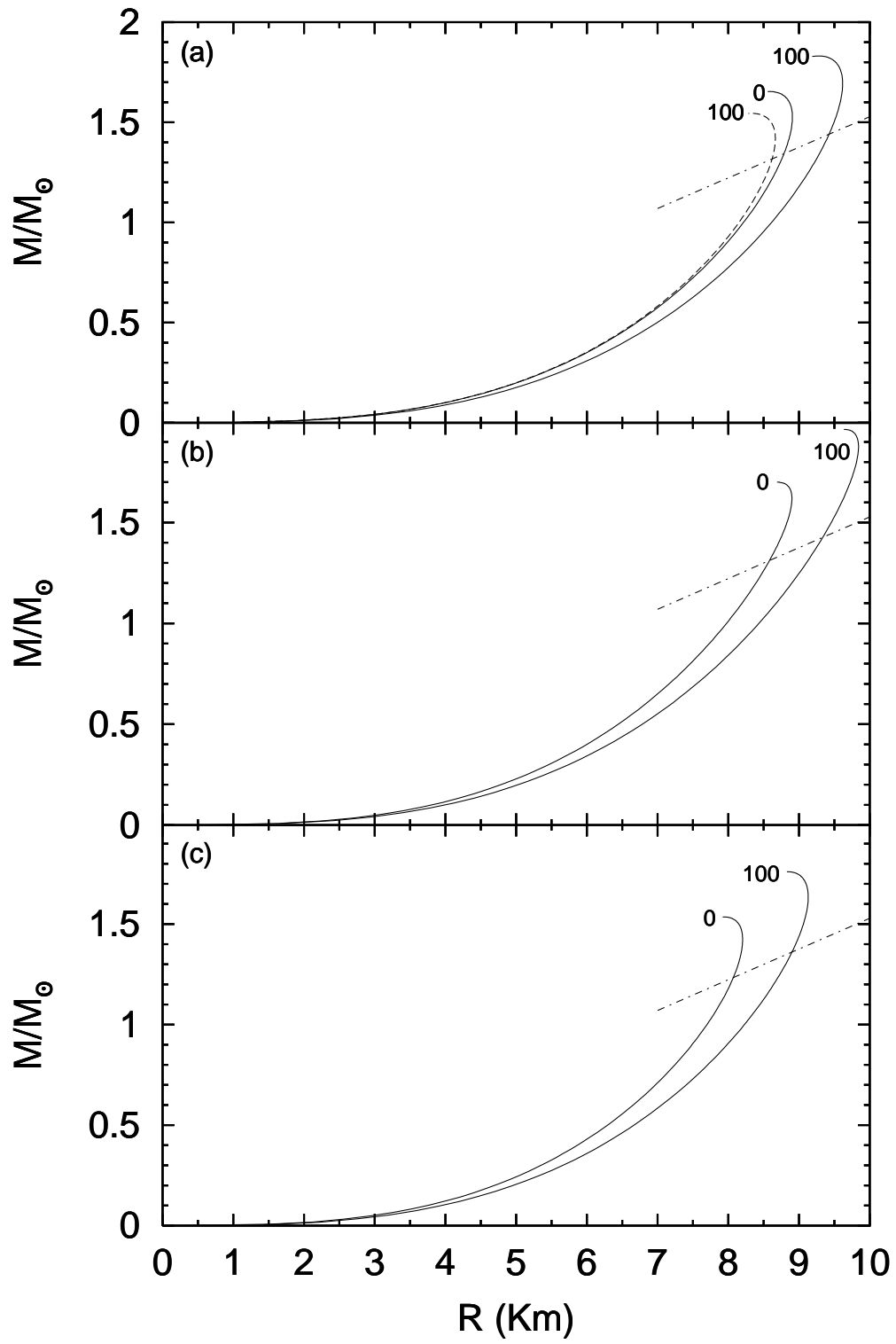


Fig. 4

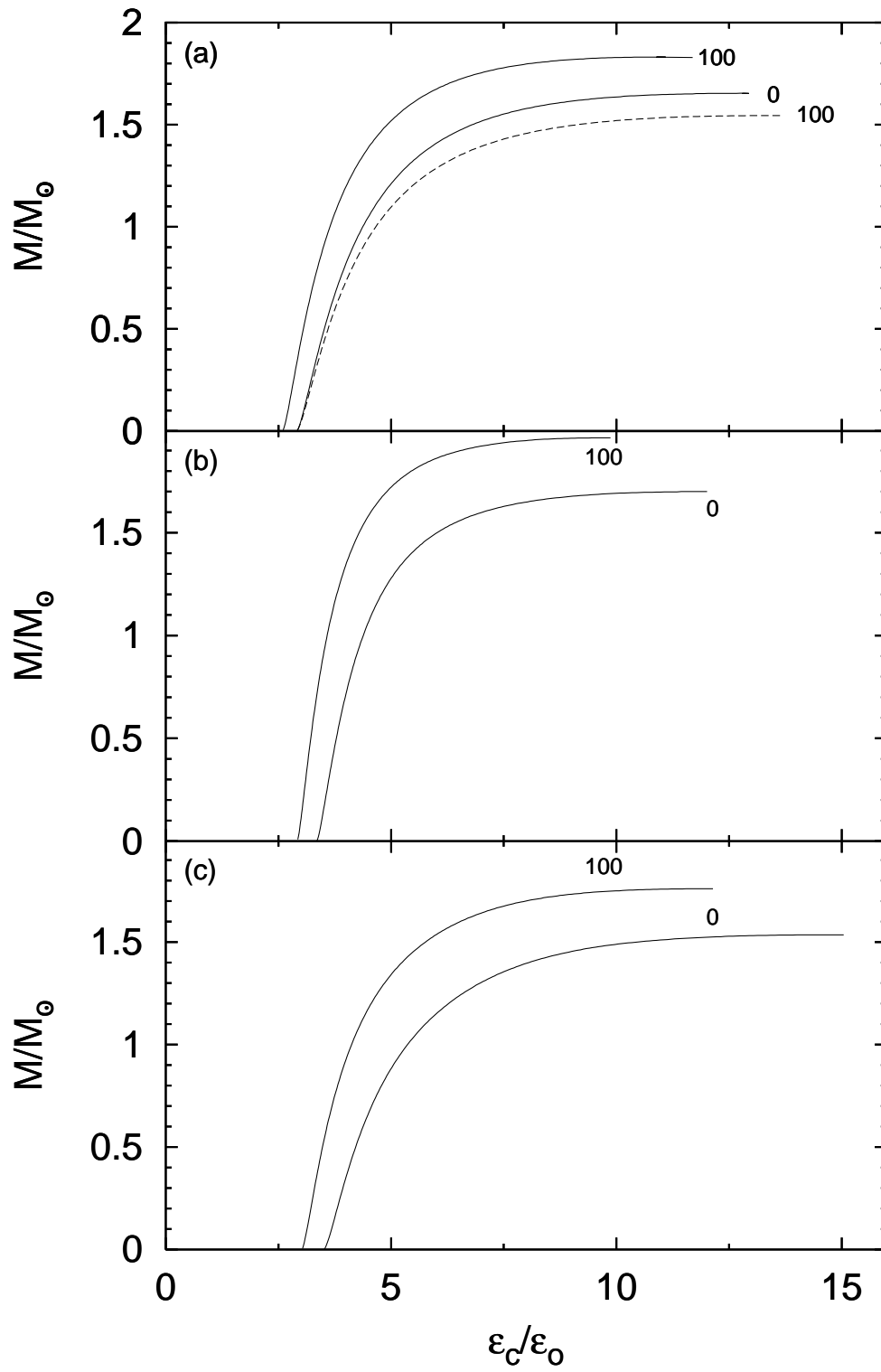


Fig. 5

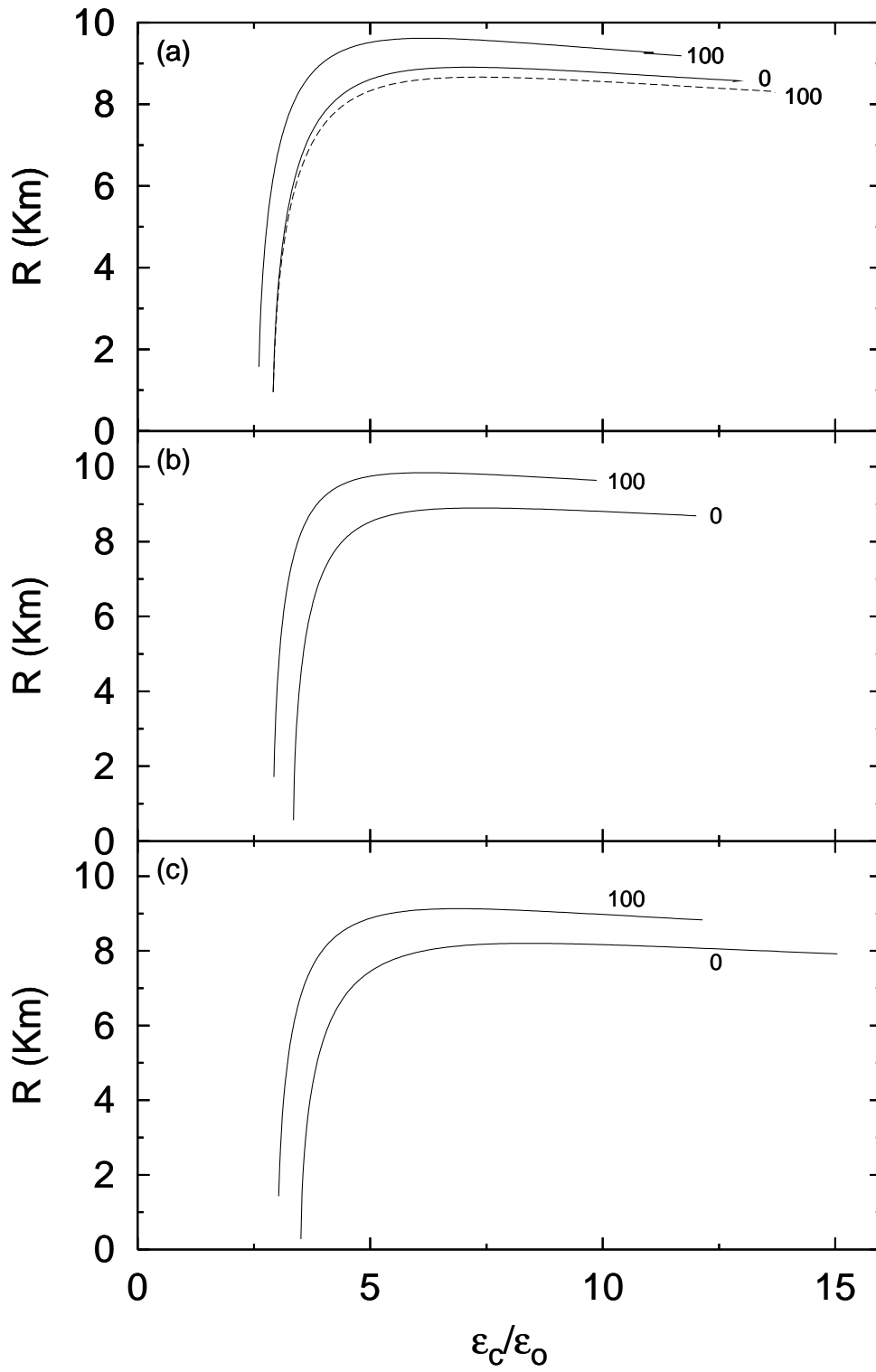


Fig. 6

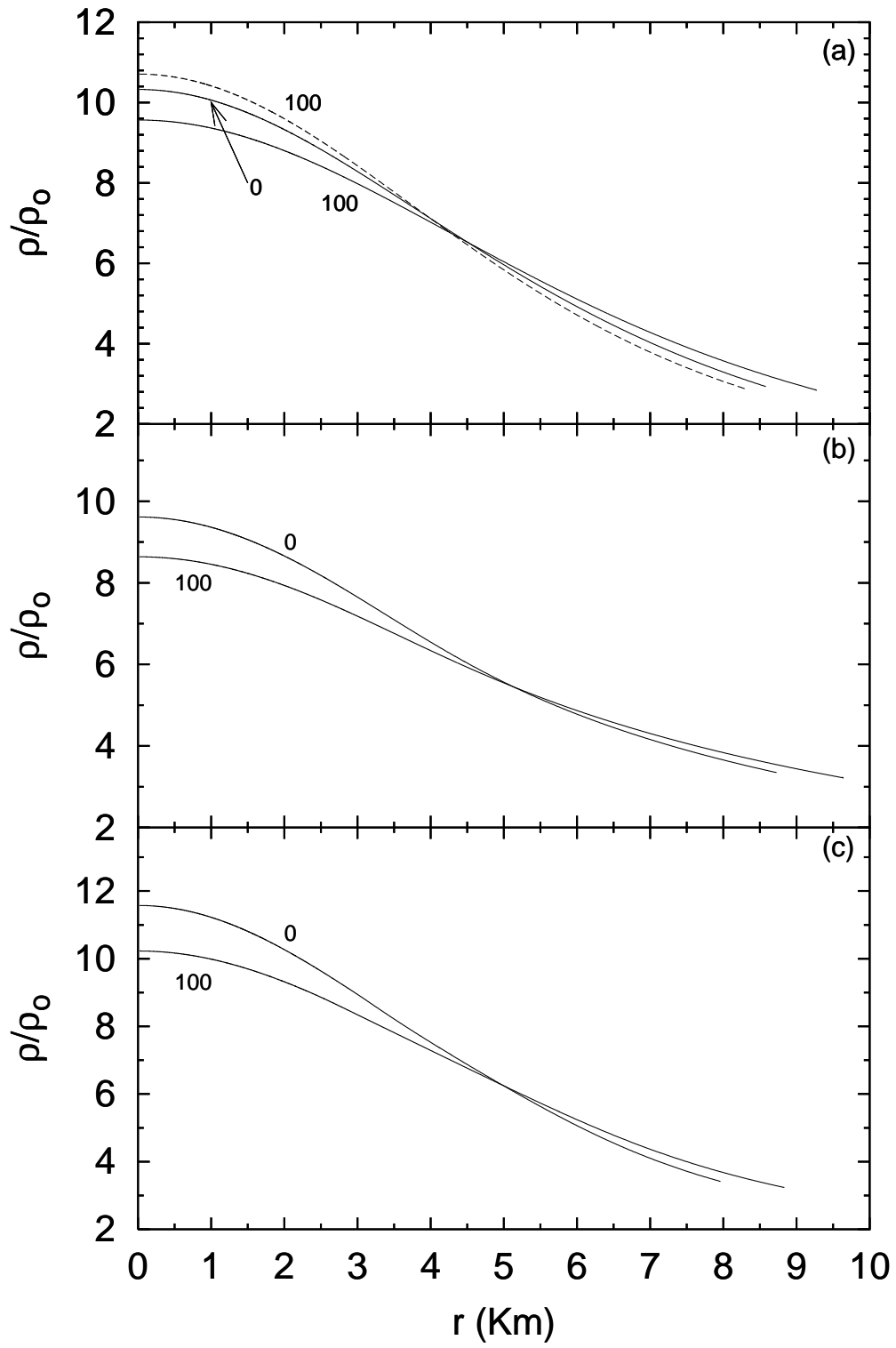


Fig. 7

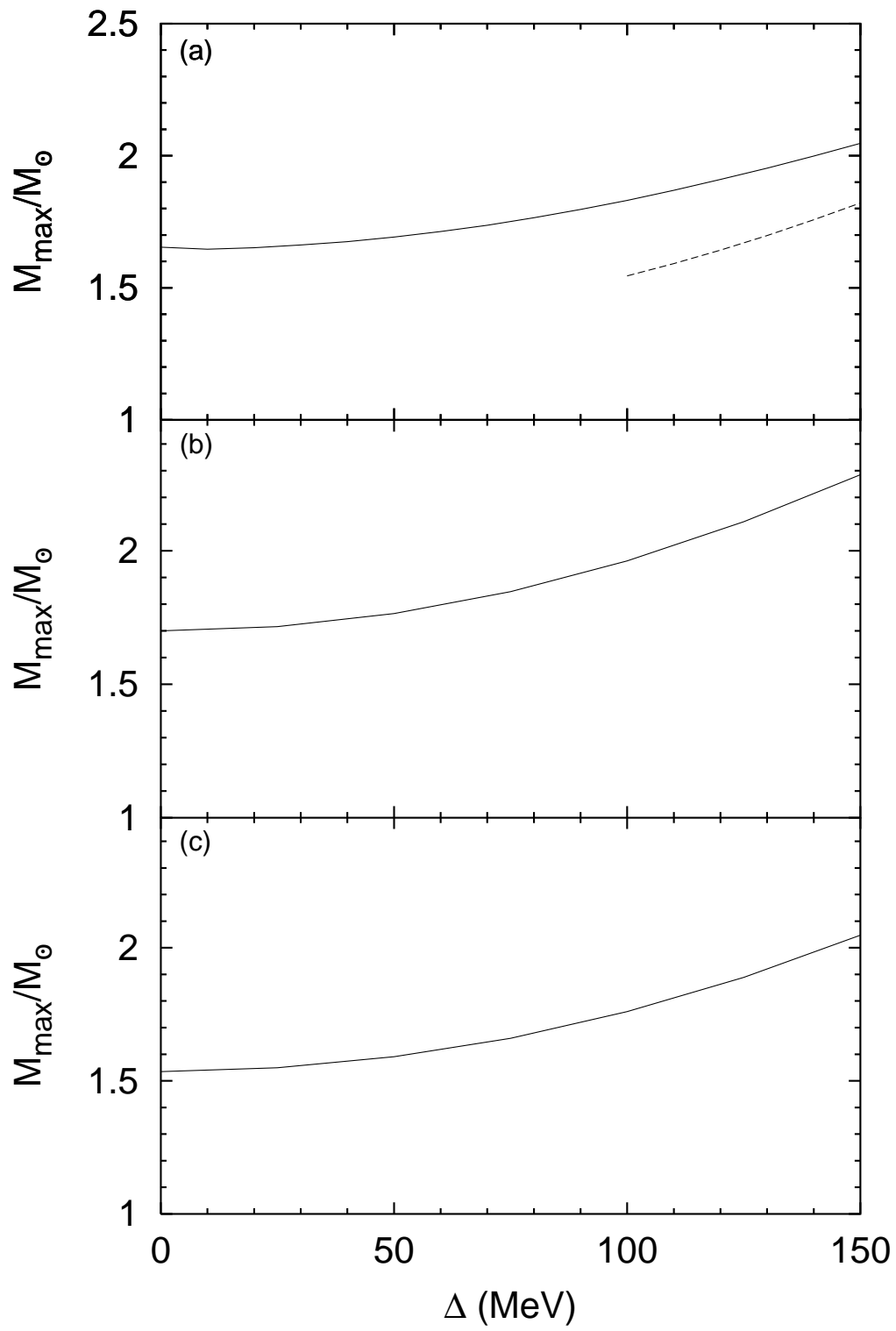


Fig. 8

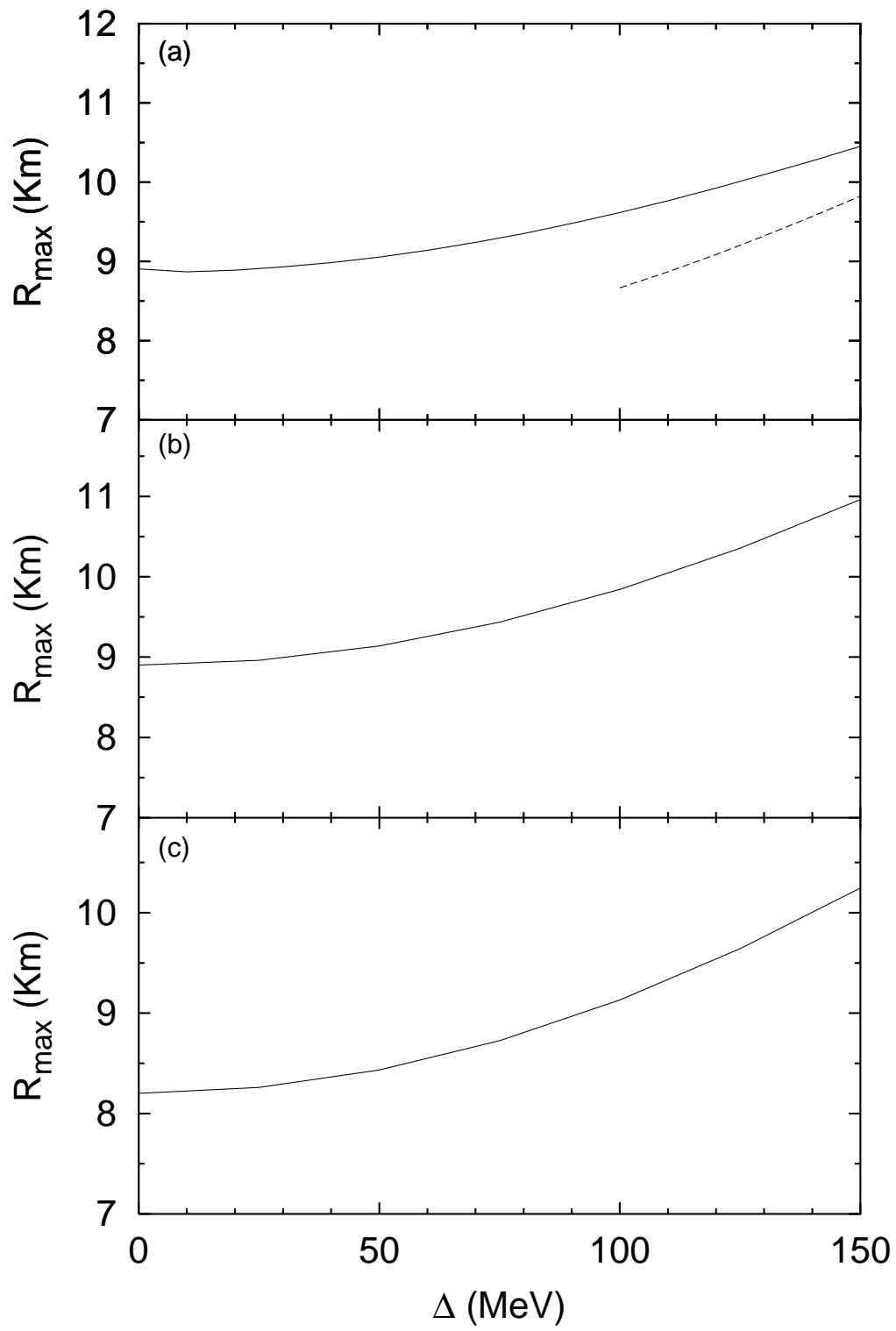


Fig. 9